Heliyon 10 (2024) e34675

Contents lists available at ScienceDirect

Heliyon

journal homepage: www.cell.com/heliyon

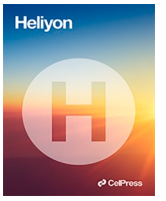

Research article

Effects during the cathode polarization of porous silicon

V. Yakovtseva [a], S. Volchek [a], V. Bondarenko [a], M.I. Sayyed [b,g], Taha A. Hanafy [c], S. Trukhanov [d], A. Bondaruk [d], A. Rotkovich [d], M.V. Silibin [e,f], T. Zubar [d], D. Tishkevich [d,*], A. Trukhanov [d]

[a] *Belarusian State University of Informatics and Radioelectronics, P. Brovka 6, Minsk 220027, Belarus*
[b] *Department of Physics, Faculty of Science, Isra University, 1162 Amman, Jordan*
[c] *Department of Physics, Faculty of Science, University of Tabuk, Tabuk, Saudi Arabia*
[d] *Laboratory of Magnetic Films Physics, Scientific-Practical Materials Research Centre of National Academy of Sciences of Belarus, 220072 Minsk, Belarus*
[e] *Institute for Advanced Materials and Technologies, National Research University of Electronic Technology "MIET", 124498 Zelenograd, Moscow, Russia*
[f] *I.M. Sechenov First Moscow State Medical University, Moscow 119435, Russia*
[g] *Department of Physics and Technical Sciences, Western Caspian University, Baku, Azerbaijan*

A R T I C L E I N F O

Keywords:
porous silicon
Cathode polarization
Surface effect
Er deposition
Oxidation
Dehydrogenation

A B S T R A C T

The large inner surface of porous silicon (pSi) not only provides unique opportunities for introducing various foreign materials into the open pores, but is also responsible for a lot of processes during the pSi cathode polarization. PSi surface and contact effects are considered in the article. The space charge layer induced by both the surface states and the double electrical layer in the solution is shown to have a decisive influence on the electrical conductivity of the silicon skeleton in the pSi layer. Depending on the depletion degree of the pSi skeleton, the electrochemical deposition of metals is possible either on the entire pSi surface or pore filling from the bottom. The erbium hydroxide formation in the process of the cathode polarization of pSi in the solution of erbium salt is shown to have a chemical nature and is stimulated by the alkalization of the cathode space. The formation of erbium-containing deposits occurs by the following mechanism. First, hydrogen is electrochemically reduced at the cathode. This causes the ion imbalance and leads to the alkalinization in the space near the cathode. The alkaline medium creates conditions for the chemical process of the erbium hydroxide formation. Formed as a gel, erbium hydroxide is physically adsorbed on the cathode surface as a film. The components of the solution are necessarily included in the deposit composition. The accompanying oxidation and dehydrogenation effects during the cathode pSi polarization are considered. Moreover, during the pSi oxidation, the solid phase extends in the pore increases the steric factor, which is essential for the formation of internal oxygen bonds. These effects are characteristic features of any pSi cathode treatment. These formation rules are true for any lanthanide. The obtained results open wide prospects for practical application of Er-filled pSi as a promising material for practical biomedical application as prospective electrodes.

* Corresponding author.
E-mail address: dashachushkova@gmail.com (D. Tishkevich).

https://doi.org/10.1016/j.heliyon.2024.e34675
Received 29 October 2023; Received in revised form 14 July 2024; Accepted 15 July 2024
Available online 23 July 2024

1. Introduction

Silicon dominates modern microelectronic technology. At the same time, other materials occupy a leading place in the production of optoelectronic, electromagnetic, and other devices. Successful integration of dissimilar materials with silicon would allow many different silicon electronic devices to be combined into a compact, reliable, and low cost system. Porous silicon (pSi) is a highly suitable material to form silicon-based composite and hybrid materials [1]. Note the difference between composite and hybrid materials. A composite material is a material consisting of two or more phases with a distinct interface. The properties of composites are usually much higher than the average characteristics of the original components that make up the composite. At the same time, hybrid materials are materials obtained by the chemical interaction of different components to form a specific (crystalline, spatial) structure that differs from the structures of the original reagents, but often inherits certain functions of the original structures [2].

Why do we choose porous silicon? PSi is a silicon single crystal penetrated by a network of numerous pores. So, a characteristic feature of pSi is the large internal surface. Depending on the porosity range, it amounts to 10–100 m^2/cm^3 for macro-PSi, 100–300 m^2/cm^3 for meso-PSi, and 300–800 m^2/cm^3 for micro-PSi [3].

PSi can be made by diverse means. Electrochemical methods of silicon etching predominate. During the anodic polarization in certain solutions, silicon dissolves. At high potentials at the anode, the silicon surface is electropolished, providing a flat smooth surface. However, at low anode potentials, a network of channels is formed that penetrates from the surface into the Si bulk. The pore formation is possible at voltages up to the electropolishing voltage. Several comprehensive books on porous silicon that provide detailed information related to silicon anodization have been published [3–7].

The pSi surface is passivated, however remains chemically highly active. The very large internal surface area offers unique opportunities for introducing various foreign substances into the open pores of pSi [3–9]. It is noticeable that pSi (as well as solid silicon itself) is a strong reducing agent capable of reducing many substances in solutions. This property is used to deposit reductively various materials onto the internal surface of pSi. The deposition of foreign substances into pSi can be made by different methods. Electrochemical or electroless metal depositions from solutions are most preferred [10]. It is noteworthy that both processes are electrochemical in nature because they are reduction reactions with charge transfer. In the electrochemical method, the redox potential is easy to change, which creates unique opportunities for oxidation and reduction processes. Metals located in the metal activity series to the right of Al are easily reduced from solutions at the pSi internal surface by a cathode polarization. Other metals, particularly the rare earth elements (REEs), are usually deposited as hydroxides [11,12]. The successful cathode deposition of metals and semiconductors (Ni, In, Ge, ZnO) into pSi has been reported [13–19].

In 1994, T. Kimura and co-workers first proposed introducing erbium into pSi by the electrochemical cathodic polarization in an erbium salt solution [20]. However, neither the processes during the electrochemical cathode deposition nor the composition of material formed have been considered by the authors. In succeeding years, a large number of papers on the study of the optical properties of pSi electrochemically doped with Er were published [21–25]. However, almost all works only report *how* (electrolyte compositions, polarization regimes, etc.) the deposition was carried out, but do not answer questions about *why* it proceeds in this particular way. Moreover, many researchers still believe that metallic erbium is reduced at the cathode surface when the cathode is polarized in the solutions of erbium salts, which is impossible in principle, since according to Pourbaix diagrams, the equilibrium electrode potential of erbium reduction reactions is −2.296 V [26]. When attempting to provide the cathode polarization up to this

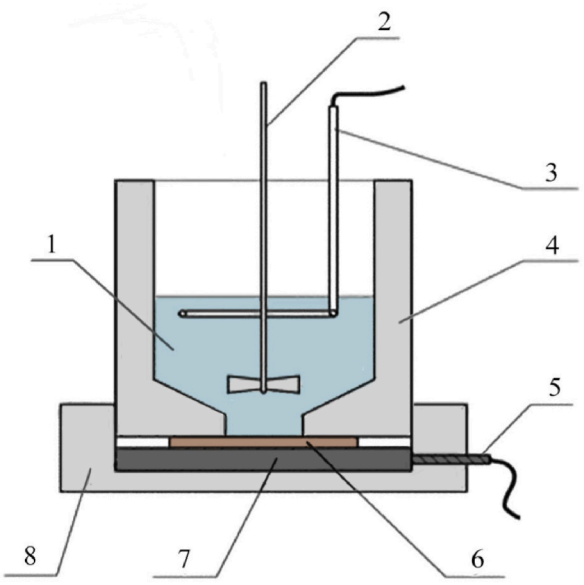

Fig. 1. The schematic of the electrochemical cell for the Si anodization: 1 – electrolyte; 2 – mechanical stirrer; 3 – Pt cathode; 4 – screw-in Teflon cylinder; 5 – current supply to anode; 6 – anode (Si wafer); 7 – graphite contact to Si anode; 8 – screw-in Teflon cylinder.

potential, the electrochemical degradation of solvents in the solutions gets ahead of the process.

Therefore, it is very important to understand the processes occurring in pSi during the cathode polarization in the solutions. When we have carried out a thorough research into the cathode polarization of pSi in the solutions of erbium salt $Er(NO_3)_3$, a number of effect were discovered. These effects are characteristic features of pSi and should be taken into account for any cathode polarization of pSi in the solutions, for example, for the cathode cleaning, cathode precipitation of foreign materials into pSi, etc.

2. Materials and methods

2.1. Porous silicon formation by anodization

As initial substrates, n^+-type (100) commercial silicon wafers with a resistivity of 0.01-Ohm·cm were used. The wafers were cut from ingots obtained by the Czochralski method that were uniformly doped with antimony to the concentration of $4{\cdot}10^{18}$ at/cm^3. The surface of silicon wafers was cleaned in a boiling ammonium peroxide solution (NH_4OH: H_2O_2: $H_2O = 1:1:3$) followed by washing in distilled water. The layer of native silicon dioxide was removed from the surface of the wafers in a 4.5 vol% solution of hydrofluoric acid. Anodizing was carried out in a non-thermostated two-electrode fluoroplastic cell with a horizontal placement of the working electrode. The cell is shown schematically in Fig. 1.

The current source was a Metrohm Autolab PGSTAT302 N potentiogalvanostat controlled by a computer. When silicon wafers were anodically polarized in the 48 % hydrofluoric acid at a current density of 10 mA/cm^2, pSi layers of a 55 % porosity were formed at the surface.

2.2. PSi cathode polarization in the solution of erbium salt

A pSi cathode polarization was carried out in the 0.1 M $Er(NO_3)_3$ solutions at the current density of 500 mA/cm^2. Ethanol (95 % C_2H_5OH +5 % H_2O) and a five-water nitrous oxide salt of erbium $Er(NO_3)_3{\cdot}5H_2O$ were used to prepare the working solution.

To determine the kinetics and peculiarities of the erbium-containing film formation, an electrochemical cell with separated anode and cathode spaces was used. The cell schematic and general views are shown in Fig. 2.

The cell consists of separate anode and cathode fluoroplastic vessels. The cathode part is the electrochemical cell with the bottom horizontal electrode arrangement. The anode part is a fluoroplastic container 2 with the working solution 3. The volume of both anolyte and catholyte was every of 10 ml. Such a ratio of volumes makes easier a quantitative assessment of results to be obtained. The anode and cathode containers are connected by a salt bridge 7. The connecting bridge between the cathode and anode spaces is a flexible polymer tube of 2-mm inner diameter equipped with 2.5-μm capillaries at both ends. The salt bridge was filled with the working solution. A plate of spectrally pure graphite served as an anode. Such a design of the cell renders impossible mixing anolyte and catholyte. The electrochemical treatment of the samples was performed in the galvanostatic regime at a 1.5 mA/cm^2 current density.

Voltammetry with both single linear and cyclic potential sweeps was used to study the electrochemical processes occurring at the electrode/solution interface. Information on the reversibility of electrochemical reactions, redox potentials of substances involved in the reactions, kinetics of charge transfer, adsorption and chemical fixation of substances can be obtained from voltammograms (VA).

At the linear sweep (with monotonic variation) of the potential, the current density in the voltammetry is the sum of the non-Faraday i_{nf} and Faraday i_f components. These current components are separated a priori as follows:

$$i = i_{nf} + i_f = C_d\frac{dE}{dt} + i_f$$

where C_d is a double layer capacitance, E is a true electrode potential, and t is time. Since the capacitance of the double layer depends on the potential, the non-Faraday component is variable. At voltage sweep rates less than 1 V-s-1, the densities of non-Faraday currents

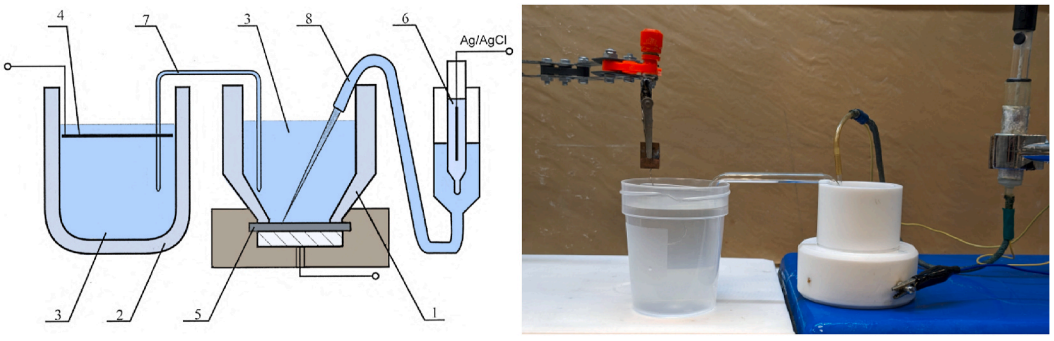

Fig. 2. The electrochemical cell with separated anode and cathode spaces: (1) cathode container; (2) anode container; (3) working solution; (4) anode; (5) cathode; (6) reference Ag/AgCl electrode; (7) salt bridge; (8) Luggin capillary system.

compared to Faraday currents are usually much lower. At high sweep rates, the non-Faraday component can become high enough to have a significant effect on the VA shape.

The Faraday current corresponds to the reduction/oxidation of the substance to be determined. The Faraday current density for a reversible cathode electron transfer process of the $O + ne \leftrightarrow R$ type is:

$$i_f = i_p + i_s$$

where i_p is the current density at the flat electrode and i_s is its sphericity correction. The Faraday current density at the flat electrode and the sweep rate of the voltage ν in the direction of the cathode are related by the equation:

$$i_p = \frac{(nF)^{3/2} c_0^0 (\nu D_0)^{1/2} W_p}{(RT)^{1/2}}$$

where c_0^0 is the concentration of O particles in the volume, D_0 is the diffusion coefficient of O particles, and W_p is an electrode potential function for which it is difficult to give an exact expression, but tables of numerical values are available [27]. The sphericity correction data also provided in this paper.

2.3. Sample evaluation

The pSi layer morphology was studied with a Hitachi S-4800 scanning electron microscope providing resolution of 1 nm. Energy dispersive X-ray spectroscopy (EDX) and the IR transmission spectroscopy were used to evaluate the elemental composition. EDX spectra were taken with a Bruker QUANTAX 200 spectrometer. The distribution of elements in the contact area was studied by the secondary-ion mass spectroscopy (SIMS) on a TOF secondary ion mass spectrometer SIMS 5 (IONTOF, Germany). The samples were etched with cesium ions at the accelerating voltage of 2 kV. The IR transmission spectra were recorded using a PERKIN-ELMER spectrometer in the wave number range of 850–2300 cm^{-1}.

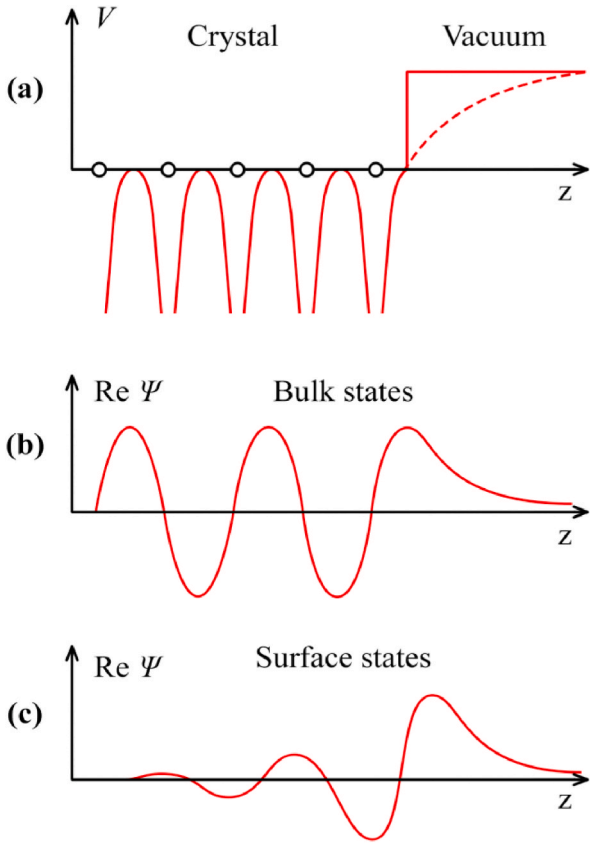

Fig. 3. (a) Potential energy distribution near the crystal surface. Wave functions of a semi-infinite (terminated on the one hand) crystal corresponding to (b) bulk and (c) surface states [29].

3. Results and discussion

3.1. PSi surface and contact effects

As mentioned above, pSi has a huge specific surface area. The famous physicist Wolfgang Pauli figuratively said about the surface: "God made the bulk; the surface was invented by the devil." Indeed, many laws for the semiconductor crystal bulk are turned out to be not applied to the description of surface properties. Most semiconductor surfaces are significantly modified compared to the corresponding atomic planes in the semiconductor bulk. Since there are no neighboring atoms on one side, the forces acting on the surface atoms change. It was experimentally established that the atoms of the surface layers of the atomically pure surface are displaced from their normal positions in the crystal lattice and rearranged into surface structures of a different symmetry. Therefore, it is absolutely clear that the structure of the surface atomic layer will differ from the structure of the corresponding atomic planes in the bulk. Special conditions for atoms on the surface compared to atoms in the crystal bulk are the breaking of the crystal translational symmetry and the formation of dangling bonds. The presence of dangling bonds on the surface is energetically very unfavorable. The surface will try to eliminate dangling unsaturated bonds. In an effort to achieve equilibrium, surface electrons will form additional bonds between atoms on the surface itself so that the number of broken bonds is significantly reduced. In particular, neighboring atoms form additional bonds with each other and combine into pairs, so-called dimers. In this case, the atoms of each dimer come closer to each other, moving away from neighboring atoms. As a result, the order of the crystal lattice on the surface changes and reconstruction occurs (i.e., a new superstructure is formed). Therefore, after the reconstruction the surface actually becomes a new "phase".

So, the silicon surface is a violation of the crystal periodic lattice. Obviously, the structure of the energy bands should also change in this case. This issue was first investigated in 1932 by I.E. Tamm [28], who theoretically predicted the existence of surface levels due to the fact that the periodicity of the potential is violated near the surface, i.e. the potential barrier of the boundary atom differs from the potential barrier of the atom inside the crystal. An one-dimensional simplified model of the crystal potential is depicted in Fig. 3a [29]. In the bulk of the crystal, the potential periodicity is equal to the lattice constant a, and near the surface it reaches the vacuum level value. In Fig. 3, the solid line shows a simplified step potential, which is mainly convenient for simple model calculations. The dashed line shows the potential at the real surface.

The breakage of the crystal lattice and the associated violation of the translational symmetry in the crystal cause the appearance of allowed energy levels in the band gap. The wave functions of electrons for these levels decay rapidly with distance from the surface, both deep into the crystal and into vacuum Fig. 3b,c. Consequently, these states are characteristic of the surface itself, and the electrons occupying them are located on the surface.

The solution of the Schrödinger equation in the surface region both for weakly bound electrons and in the case of a strong bond leads to the conclusion that, in addition to the usual energy bands, there are surface energy states of electrons. These additional levels should be acceptor ones because the surface atoms have incomplete electron shells, since they have three neighboring atoms instead of four (Fig. 4.). Therefore, the surface of the silicon wafer will have p-type conductivity.

The density of surface levels called as surface states should be of the same order as the number of atoms per unit of the crystal surface, i.e., about 10^{15} cm^{-2}. This density is very high, so the hole electrical conductivity of the silicon surface should be strongly pronounced.

However, the real silicon surfaces have a much more complex structure than the model proposed by Tamm with a simple break in the periodicity of the crystal lattice. The real semiconductor surfaces are always covered with a layer of adsorbed or chemically bonded atoms and molecules. Fig. 5 [30] shows a representative example of a cluster Si_9H_{12} used as a model for describing the Si(100) surface. At the ideal surface, there are two broken Si–Si bonds for every surface atom. The number of dangling bonds corresponding to

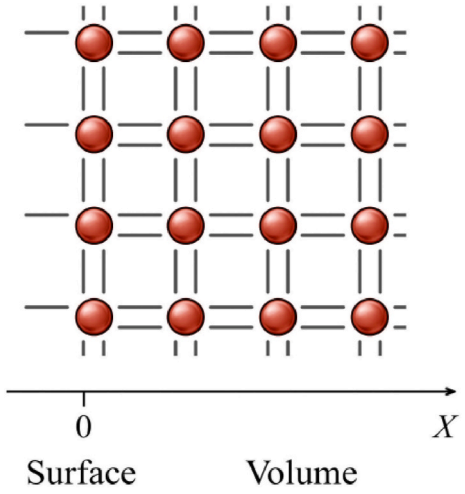

Fig. 4. Schematic representation of an ideal as yet non-reconstructed Si surface.

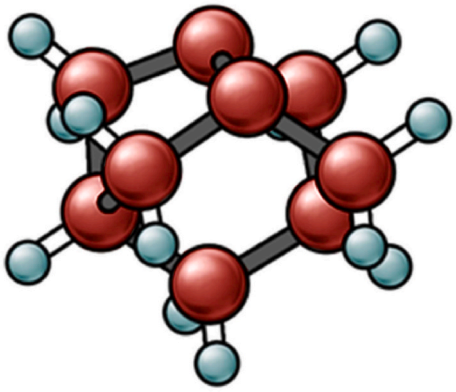

Fig. 5. Si_9H_{12} cluster used as a model to describe a Si(100) surface [30]. The large balls correspond to silicon atoms and the small balls represent hydrogen atoms. (For interpretation of the references to colour in this figure legend, the reader is referred to the Web version of this article.)

unsaturated orbitals is reduced by the surface reconstruction through the creation of Si dimers at the surface. The dangling silicon bonds in the cluster can be saturated with hydrogen atoms. It should be mentioned that the pSi reactivity is dictated by the chemistry of Si–H and Si–Si bonds, both being strong reducing agents that can reduce water to hydrogen [31,32]. A mixture of Si–H, SiH_2, and SiH_3 species are included in the pSi surface [33].

So, the surface levels induced by adsorbed atoms and various surface defects play a decisive role on the real surface. The energy position of the surface level formed due to the foreign atom adsorption or surface defects depends both on the lattice parameters and on the properties of the adsorbed atoms or defects. A theoretical consideration of the problem of the surface states caused by adsorbed atoms showed that under certain conditions the adsorbed atom creates an energy level inside the band gap. When the adsorbed atom

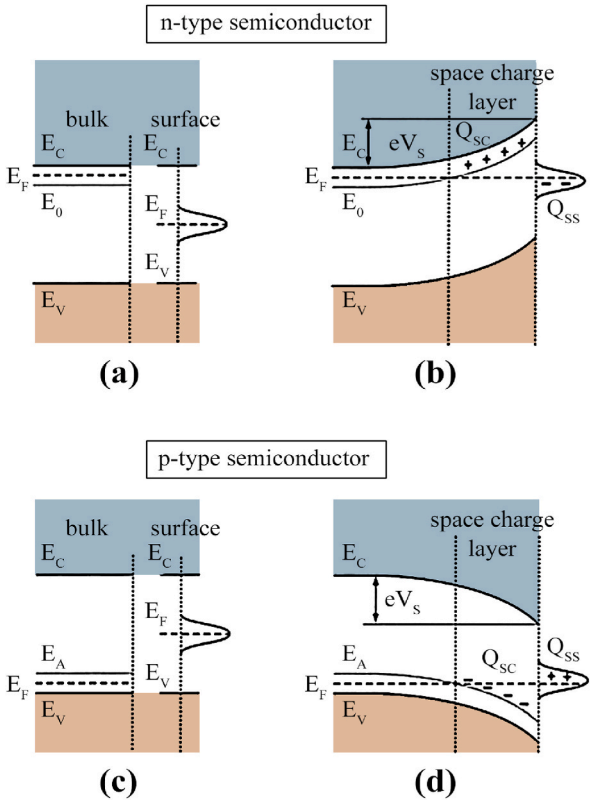

Fig. 6. Band bending at the surface of (a, b) n-type and (c, d) p-type semiconductors; (a) and (c) show the disequilibrium between the Si bulk and surface. (b) and (d) illustrate the band bending in the equilibrium state; E_c and E_v are the edges of conduction and valence bands, E_F is the Fermi energy, E_D and E_A are the energies of the bulk donor and acceptor levels. $Q_{ss} = -Qsc$ are the charges at the surface and in the space charge layer. $eV_s = ev$ ($z = 0$) indicates the band bending [adapted from reference 29].

moves away from the surface, this local surface level is pulled up to the conduction band and disappears in the limit.

The surface states can be either donors or acceptors. Filling of acceptor levels means the localization of electrons, the removal of electrons from the donor levels means the localization of holes. As a result of these processes, the surface is charged with negative or positive charge. The charge due to surface states disrupts the electronic structure inside the semiconductor. Since at standard conditions the semiconductor crystal should be electrically neutral, the surface charge is compensated by an equal and opposite charge in the near-surface layer. Neutralization occurs due to the attraction to the surface of charge carriers with a sign opposite to the sign of the surface charge, and the repulsion of charge carriers of the same sign. Therefore, the near-surface layer of the semiconductor turns out to be depleted of charge carriers having the same sign as the surface charge, and enriched with carriers of the opposite sign. Thus, the surface layers enriched with carriers are formed, and a potential difference (the surface potential) ϕ_s arises between the surface and the bulk. This parabolic surface potential (Fig. 6) leads to the distortion (bending) of energy levels near the surface. Fig. 6 also illustrates band bending at the surface of (a, b) n-type and (c, d) p-type semiconductors; (a) and (c) show the disequilibrium between the Si bulk and surface. (b) and (d) illustrate the band bending in the equilibrium state; E_c and E_v are the edges of conduction and valence bands, E_F is the Fermi energy, E_D and E_A are the energies of the bulk donor and acceptor levels. $Q_{ss} = -Qsc$ are the charges at the surface and in the space charge layer. $eV_s = ev$ ($z = 0$) indicates the band bending.

The thickness of the space charge layer, during which the surface charge is neutralized, depends on the concentration of charge carriers in the semiconductor. It is usually taken to be equal to the so-called Debye screening length L_D. The Debye length has the following meaning: L_D is the distance over which the field potential in a substance with free current carriers decreases by a factor of *e*. The calculation shows that

$$L_D = \left(\frac{\varepsilon_0 \varepsilon_s kT}{q^2 n_1}\right)^{1/2}$$

where ε_0 is the dielectric constant of vacuum; ε_s is the dielectric constant of the semiconductor; k is Boltzmann's constant, T is the absolute temperature, q is the electron charge, n_1 is the concentration of charge carriers in the intrinsic semiconductor [34].

As a result, the surface layer is depleted in carriers of one sign and at the same time enriched in carriers of another sign compared to the bulk layers. The concentration of electrons and holes in the near-surface layer is described by the general relations

$$n = n_i \exp\frac{E_F - E_i}{kT}; p = p_i \exp\frac{E_i - E_F}{kT}$$

where E_i is a middle of the band gap, E_F is the Fermi level. The Fermi level at the semiconductor surface is always in the middle of the band gap. So, if in the near-surface layer the middle of the band gap is located below the Fermi level, the semiconductor near the surface behaves like an n-type semiconductor, since in this case $n > n_i > p$. Accordingly, if in the near-surface layer the middle of the band gap is located above the Fermi level, the semiconductor changes the sign of the charge, i.e. becomes as if a hole semiconductor. Charge-induced bending of the bands on the surface results in an increase in the distance from the Fermi level to the conduction band bottom in n-type semiconductors and to the valence band top in p-type semiconductors. At the point of contact between the surface and the bulk, electrons from the higher level move to unoccupied lower levels until the Fermi levels in the bulk and on the surface become equilibrium (Fig. 6).

Let us consider what happens when pSi is placed in an electrolyte. The semiconductor-electrolyte interface is of great importance in electrochemical reactions. Electrolytes are conductors of the second kind, the electrical conductivity of which is due to the movement of positively charged cations and negatively charged anions in the solution. The decomposition of the electrolyte into ions (dissociation) occurs only in solvents whose molecules are polar, for example, in water. Water molecules are strongly bound together by H-bonds. To dissolve apolar substances in water, the H-bonds must be broken, which is energetically unfavorable. To minimize energy loss, water molecules will still try to form as many H-bonds as possible with apolar molecules. But water is the most polar liquid. Water molecules are dipoles and interact electrostatically with solute ions, forming solvated cations and anions, shown schematically in Fig. 7. This gives a certain arrangement of water structure around the apolar molecules, which results in a reduction of entropy. Therefore, water layers in close proximity to apolar molecules have relatively low entropy.

So, the solute molecule is surrounded by a solvate shell, consisting of more or less closely bound solvent molecules. A certain amount of energy is released in the process of solvation.

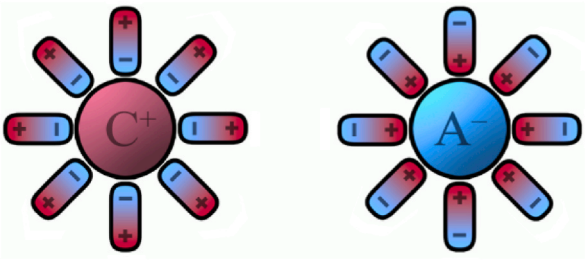

Fig. 7. Solvated cations and anions.

The pSi/solution interface represents a double electrical layer consisting of an electrical charge on the pSi surface and a charge of ions in the solution at a short distance from the pSi surface. This double layer is generated as a potential is applied to pSi and a charging current (non-faradic current) flows through the cell.

The half of the double layer located in the solution can be visualized as consisting of separate sub-layers (Fig. 8). The first layer is composed of the specifically adsorbed solvent molecules and desolvated ions. The location of the electric centers of this layer represents the boundary of the inner plane of the Helmholtz layer and is located at a distance χ_1 from the pSi surface. Solvated ions constitute the second layer. Being completely surrounded by the solvent molecules, these ions cannot come closer than χ_2, and the location of the electric centers of these ions represents the outer plane of the Helmholtz layer. The interaction of solvated (non-specifically adsorbed) ions with the pSi surface consists only in long-range electrostatics. The ions in this plane are less compactly arranged than in the inner plane of the Helmholtz layer and are distributed in a diffuse layer that extends deep into the solution.

The pSi half of the double layer may be outlined as follows. The charge in the Helmholtz layer is compensated by the supply or removal of electrons in the pSi surface layer to a depth of about 10 thousand monolayers of the crystal lattice. In real situation, the width of this layer depleted with majority carriers (space charge layer) is much larger, since the distribution of charges occurs diffusely, according to the exponential law [35,36]. For example, for n-type semiconductor the depletion layer width, W, can be calculated from the following relation, knowing the values of V_{fb} and N_D:

$$W = \left[\frac{2\varepsilon_0 \varepsilon_s \left(V - V_{fb} - \frac{kT}{e} \right)}{eN_D} \right]^{1/2}$$

where ε_0 is permeability; ε_s is dielectric constant of semiconductor; e is the charge of electron; N_D is the donor density; k is Boltzmann constant; T is absolute temperature; V is the electrode potential; V_{fb} is the flat band potential.

The space charge layer has a decisive influence on the electrical conductivity of the elements of the silicon skeleton in the pSi layer and the pSi layer as a whole. There are several possible cases of the electrical state of the silicon skeleton between the pores. We have already determined that both surface states and the double electrical layer determine the thickness of the space charge layer in semiconductor. Fig. 9 illustrates the electrical conductivity of porous silicon skeleton elements as their width decreases. For macroporous silicon (Fig. 9a), the width of the skeleton elements range from 0.5 to 1.5–3 μm. This means that space charge layer layers even 0.1 μm thick will not have a significant effect on the electrical conductivity of the skeleton. The skeleton will be practically undepleted. The width of the skeleton elements in mesoporous silicon is in the range of 30–150 nm. The skeleton of such pSi will be partially depleted (Fig. 9b). For microporous silicon with the skeleton element width less than 2 nm and mesoporous silicon with the width of the skeleton elements less than 30 nm, the full depletion of the semiconductor skeleton is observed (Fig. 9c). At such dimensions, the space charge layers on the opposite walls of the skeleton overlap. In this case, the porous silicon skeleton practically turns into dielectric due to the absence of charge carriers. The considered cases of the conductivity state of the pSi skeleton manifest themselves most clearly during the electrochemical deposition of metals into the pore channels.

Fig. 10 illustrates the pore filling with metal during the pSi cathode polarization in suitable electrolytes for cases of various widths of the silicon skeleton.

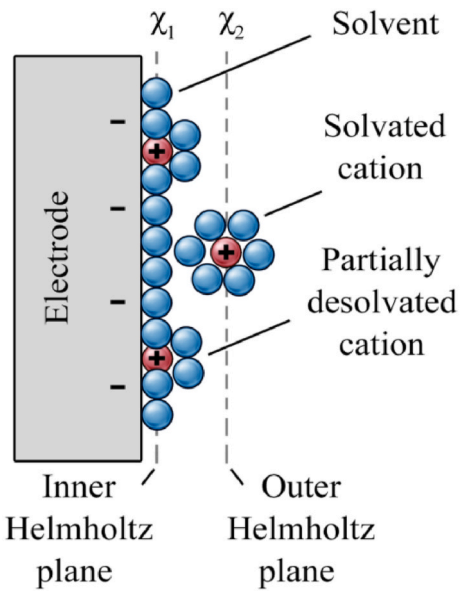

Fig. 8. Double electric layer at the pSi/solution interface (adapted from Ref. [30]).

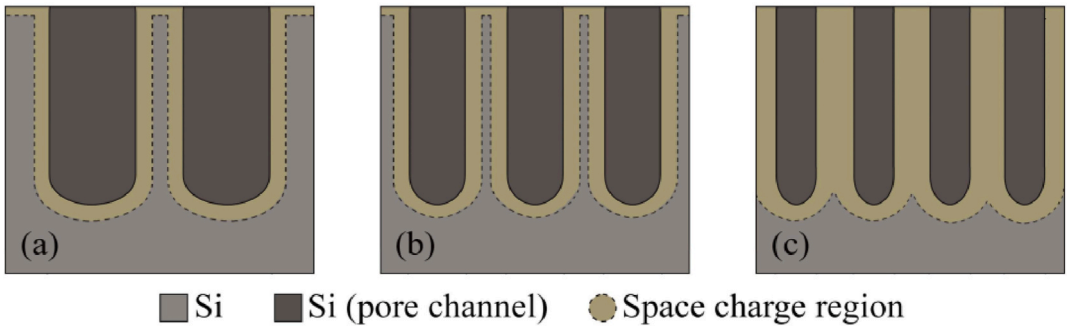

Fig. 9. The electrical conductivity of pSi skeleton elements depending on their width.

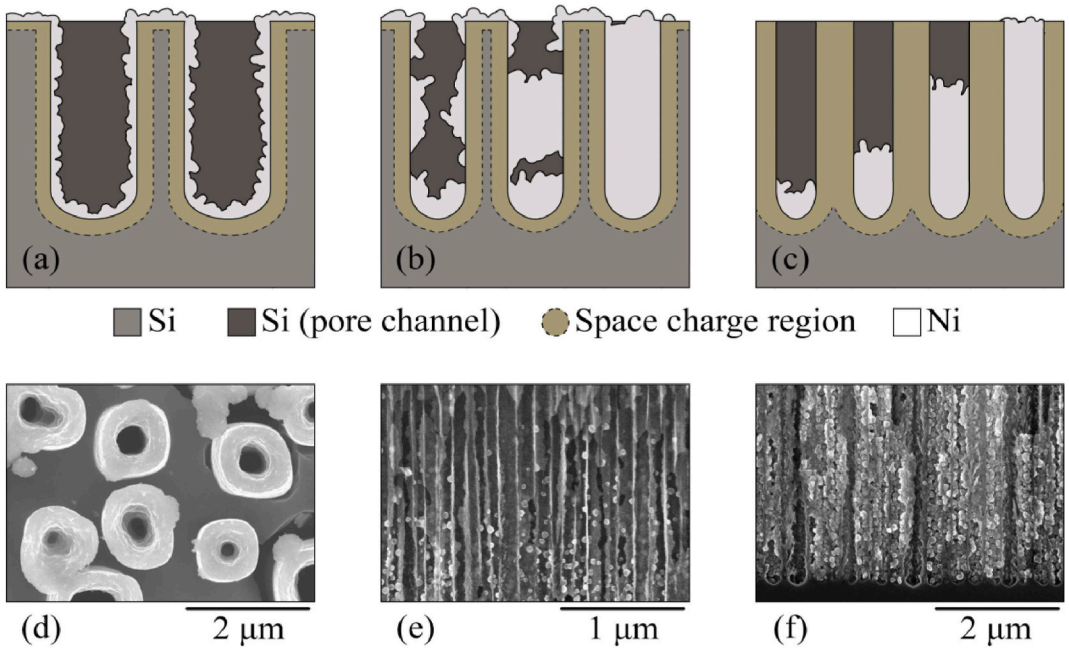

Fig. 10. The pore filling with metal during the cathode polarization of pSi depending on the width of the pSi skeleton elements: (a) pSi skeleton is partially depleted and metal is deposited on the skeleton walls, (b) pSi skeleton is partially depleted and pore channels are filled with metal, (c) pSi skeleton is completely depleted and pore channels are filled with metal, (d) SEM image of macroporous pSi with metal tubes formed by the electrochemical metal deposition, (e) SEM image of a cross section of mesoporous pSi with metal nanoparticles deposited on the surface of silicon skeleton, (f) SEM image of a cross section of mesoporous pSi with metal nanowires formed by the electrochemical deposition of metal. (For interpretation of the references to colour in this figure legend, the reader is referred to the Web version of this article.)

If the silicon skeleton of pSi is undepleted or partially depleted of charge carriers, metal particles nucleate over the entire geometric skeleton surface, including top, side, and pore bottom surfaces. Next, the metal particles are combined into a thin film covering the skeleton (Fig. 10a and b). The difference between the electrochemical deposition of metals into macro- and mesoporous silicon is only that in the first case, a metal tube is formed inside the pore, while in the second, the formation of metal columns is possible. SEM images of the corresponding structures favours this view (Fig. 10d and e). The SEM image of a cross section of mesoporous pSi with metal nanowires formed by the electrochemical deposition of metal is shown in Fig. 10f.

When the current is passed through the structure shown in Fig. 10c, only the pore bottoms remain electrochemically active, while the rest of the Si skeleton surface is excluded from the electron exchange reactions with the solution. This case is confirmed by the following our study. Fig. 11 shows voltammograms for the cathode polarization of single-crystal and microporous silicon in an aqueous 0.1 M $Er(NO_3)_3$ solution. As can be seen from Fig. 11, at the equal polarization potentials, almost half the current flows through pSi compared to single-crystal silicon. This indicates that the electrochemically active area in porous silicon is indeed smaller than both the geometric surface area of pSi and the surface area of monocrystalline silicon.

This means that complete depletion of the pSi skeleton stimulates the initiation of the electrochemical deposition from the pore bottoms and enables complete pore filling with metal. The SEM image of the structure (Fig. 10f) confirms this statement.

Thus, the pSi formation with various sizes of the Si skeleton makes it possible to control the space charge layer in the silicon

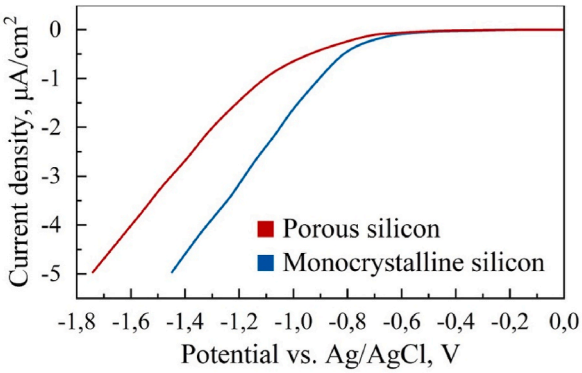

Fig. 11. Voltamograms of single-crystal and porous silicon in aqueous $Er(NO_3)_3$ solution. (For interpretation of the references to colour in this figure legend, the reader is referred to the Web version of this article.)

skeleton of the porous matrix and, as a result, to choose the deposition option depending on the required conditions.

3.2. Cathode polarization of pSi in the Er(NO3)3 solution

Like any electrochemical process, the cathode deposition follows the basic principles of electrochemical kinetics based on Faraday's and Fick's laws as well as the theory of sequential and parallel reactions. The electrochemical deposition involves the reduction of metal ions dissolved in the electrolyte at the cathode surface. As noted above, metals in the series of metal activity, located to the right of Al, are readily reduced from the solutions during the pSi cathode polarization [15,37–39]. However, as mentioned above with reference to Pourbaix diagrams [26], the electrochemical reduction of metallic erbium from salt solutions is practically unfeasible, since the attempt to reach the equilibrium electrode potential for erbium reduction of −2.296 V is outpaced by the electrochemical destruction of solutes in solutions. Indeed, the electrochemical stability of water and light alcohol is limited by processes of direct electrolysis and a cathode hydrogen reduction, and corresponding potentials are within -(1–1.5) V [40]. Therefore, the electrochemical cathode reduction of Er from the solutions is seemed to be impossible.

Let us consider the reactions involved in the electrochemical cathode treatment of the pSi electrode in the 0.1 M alcohol solution of $Er(NO_3)_3$. The solution consists of ethyl alcohol (95 % C_2H_5OH + 5 % H_2O) and five-water erbium nitrate $Er(NO_3)_3{\cdot}5H_2O$. When dissolved in water, erbium nitrate as a salt of a strong acid HNO_3 dissociates into positively charged Er^{3+} ions and negatively charged NO^{3-} ions:

$$Er(NO_3)_3 \rightleftarrows 3NO_3^- + Er^{3+}$$

The ethyl alcohol electrolysis proceeds by the following reaction:

$$C_2H_5OH + 2\bar{e} \rightleftarrows H_2 + 2C_2H_5O^-$$

One-step dissociation of water as a weak amphoteric electrolyte takes place in the solution:

$$H_2O \rightleftarrows H^+ + OH^-$$

Fig. 12 shows cyclic VAs of pSi in the working solution taken at various potential sweep rates.

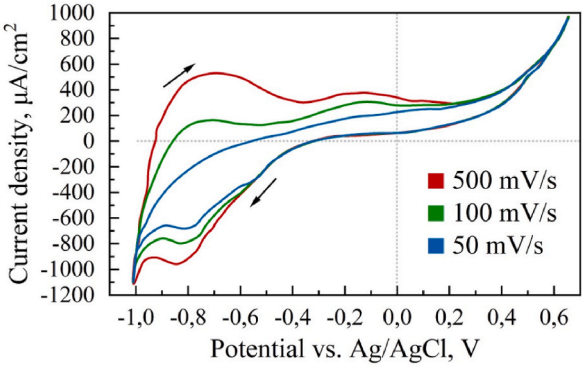

Fig. 12. Cyclic voltammograms of pSi in the 0.1 M alcohol solution of $Er(NO_3)_3$ salt at various potential sweep rates.

Referring to Fig. 12, in the direct branches of the VA a current peak at the potential of −800 mV is observed. The peak amplitude increases with the increase in the potential sweep rate. As calculations have shown, the amplitude of this peak is proportional to the square root of the potential sweep rate. This is typical for reversible reactions [41]. Since the electrolyte does not contain any cations other than hydrogen and erbium, these peaks are logically associated with the hydrogen reduction by the discharge and adsorption of atomic hydrogen according to the reaction:

$$2H^{+} + 2\bar{e} \rightarrow 2H^{0} \rightarrow H_2\uparrow$$

At higher potentials, molecular hydrogen is reduced at the cathode by the reaction:

$$H^{0} + H^{+} + \bar{e} \rightarrow H_2\uparrow$$

The depletion of H^{+} ions takes place in the cathode region in the process, while an excess of OH^{-} groups is observed in the solution. That is, the solution is alkalized in the cathode space. The solution alkalinization promotes the chemical reaction of the erbium hydroxide formation, because in the solutions with pH = 6.8–7.5 the chemical reaction of the lanthanide hydroxide $Ln(OH)_3$ formation is typical for all lanthanides [41]:

$$Er^{3+} + OH^{-} \rightleftarrows (ErOH)^{2+}$$

In addition, there appears to be an excess of alcohol radicals relative to H^{+} hydrogen ions. In addition, there appears to be an excess of alcohol radicals relative to H^{+} hydrogen ions. In this case, a reaction of Er^{3+} ions bonding with the alcohol radical takes place. Since this reaction proceeds without the involvement of electrons, it is a purely chemical reaction rather than an electrochemical one:

$$C_2H_5O^{-} + Er^{3+} \rightarrow Er(C_2H_5O)_3$$

This reaction propagates from the immediate surface of the cathode to the solution at some distance. It is clear that the concentration of erbium-containing molecules is maximum at the electrode surface and decreases with distance from the electrode into the solution. Typically, hydroxides of any lanthanides $Ln(OH)_3$ appear as amorphous gels [42]. Such a gel is formed in PSi when a sufficient number of erbium-containing molecules are formed. Being physically adsorbed on the pore sidewalls, this gel forms erbium-containing deposit.

Fig. 13 shows the elemental composition of the pSi after the cathode treatment in the 0.1 M alcohol solution of $Er(NO_3)_3$ evaluated by EDX.

As evident from Fig. 13, gel contains a significant amount of erbium. Fig. 14 shows the SIMS spectrum of the sample. As shown in Fig. 14, erbium, oxygen, and carbon are detected throughout the film thickness in significant amounts. Since the samples were sputtered with nitrogen ions during the SIMS spectra recording, the nitrogen distribution profiles in the deposit are not given. Carbon in the SIMS spectrum confirms the presence of the alcohol radical (C_2H_5O) in the composition of the erbium-containing deposit.

Thus, it was revealed that the cathodic polarization of pSi in the $Er(NO_3)_3$ alcohol solution resulted in the formation of the erbium-containing deposit, which contains contains Er^{3+}, OH^{-}, and NO_3^{-} groups and the alcohol radical $C_2H_5O^{-}$. The composition of the deposit can be summarized as $Er(OH)_x(NO_3)_y(C_2H_5O)_z{\cdot}nH_2O$. Because the oxidation degree of erbium in the compounds is 3+, the stoichiometric coefficients equal $x + y + z = 3$.

It should be noted that replacing the alcohol solution with an aqueous one leads to the formation of a gel of the following composition:

$$Er^{3+} + OH^{-} + NO_3^{-} \rightarrow Er(OH)_x(NO_3)_y$$

where $x + y = 3$. At low current densities, the ion unbalance is negligible and NO_3^{-} groups is a considerable fraction of the deposit ($x \approx y$). When the current density increases, a fraction of OH^{-} groups in the space at the cathode increases. This results in formation of the

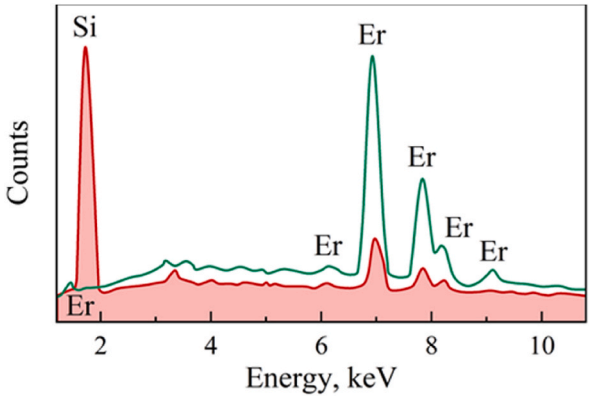

Fig. 13. EDX spectrum of pSi after the cathode treatment in the 0.1 M alcohol solution of $Er(NO_3)_3$.

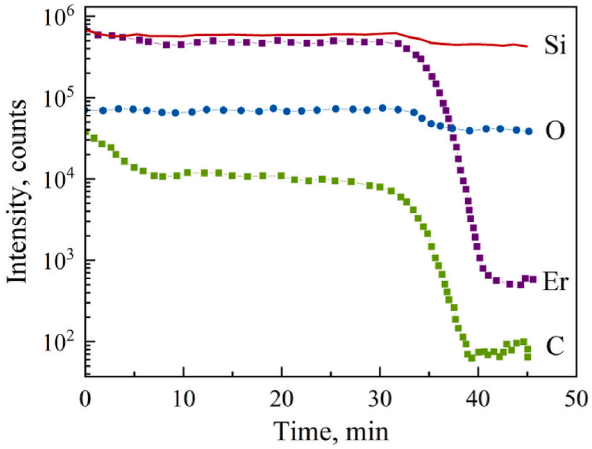

Fig. 14. SIMS depth profiling the erbium-containing deposit.

deposit with negligible content of NO_3^- groups (x → 3, y → 0).

The following mechanism of the erbium-containing deposit formation during the cathode polarization of pSi in the solution of erbium salt is proposed. First, the *electrochemical* process of the cathode reduction of hydrogen takes place. This process leads to the ion imbalance in the cathode space, creating its alkalinization. The alkaline medium promotes the *chemical* reaction of the erbium hydroxide formation. Formed as a gel, erbium hydroxide is physically adsorbed on the cathode surface as a film. The components of the solution are necessarily included in the deposit composition. There is no doubt that the character of Er^{3+} ion bonding with NO^{-3}, OH^- and $C_2H_5O^-$ groups, as well as with water molecules recorded in IR spectra, can be different: ionic, covalent, etc. Water detected as a part of the deposit may be both crystalline hydrate and accluded water. These issues are the subject of a special study.

The following experiment was a direct confirmation of the described mechanism. Dielectric paper fibers were introduced into the working solution before the cathode treatment. The fibers were randomly distributed in the solution. After the cathode treatment, the fibers located at the surface of the porous silicon sample (in the near-cathode space) were also covered with a gel-like precipitate, despite the fact that they are electrically neutral. The fibers in the solution thickness outside the Gui-Helmholtz layer remained unchanged. Thus, this experiment shows that the precipitate is deposited not only on the charged surfaces, but also on electrically neutral surfaces that are electrically unconnected to the cathode.

The above-described rules of the Er-containing hydroxide deposit formation are true for any lanthanide [12].

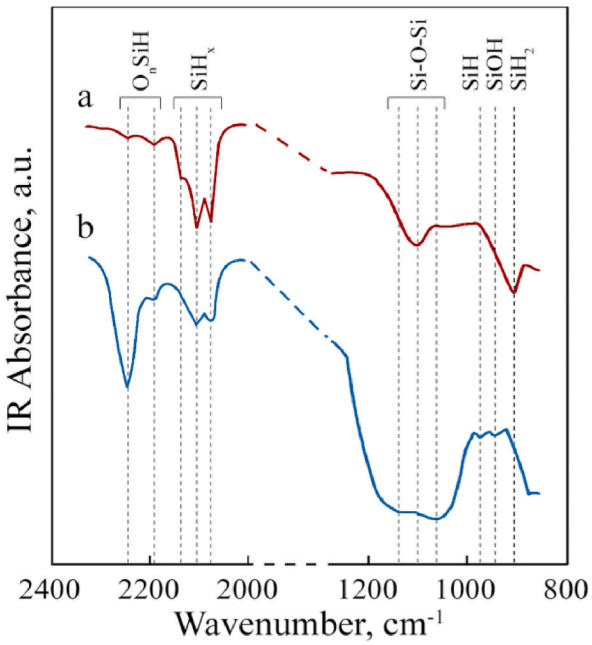

Fig. 15. IR spectra of pSi: (a) as-prepared; (b) cathodically polarized in the 0.1 M ethanol solution of $Er(NO_3)_3$.

3.3. Effects of cathode oxidation and dehydrogenation of porous silicon

The accompanying effects of cathode oxidation and dehydrogenation of pSi occurring during cathode polarization of pSi are revealed.

Fig. 15 shows the IR transmission spectra of as-prepared pSi (a) and pSi cathodically polarized in the 0.1 M ethanol solution of Er (NO3)3 (b). As can be seen from Fig. 15, the spectrum of as-prepared pSi contains valence vibrations of SiH, SiH_2, and SiH_3 groups (wave numbers of $\nu_1 \sim 2080$ cm^{-1}, $\nu_2 \sim 2105$ cm^{-1}, and $\nu_3 \sim 2130$ cm^{-1}) and deformation oscillations of SiH and SiH_2 (wave numbers of $\nu_4 \sim 970$ cm^{-1} and $\nu_5 \sim 905$ cm^{-1}). A band characteristic of stretching vibrations of the surface siloxane groups of Si–*O*–Si is observed at $\nu 6 \sim 1100$ cm-1, indicating a slight oxidation of the pSi surface.

As can be seen from Fig. 15b, after the 20-min cathode polarization of pSi in the $Er(NO_3)_3$ ethanol solution, the strong doublet transmission band of O_2SiH and O_3SiH groups ($\nu_7 \sim 2190$ cm^{-1} and $\nu_8 \sim 2240$ cm^{-1}) appears in the spectrum. This band is indicative of the reverse pSi oxidation with the formation of internal oxygen bonds. At the same time, the SiH_x transmission bands are attenuated and the deformation vibrations of SiH groups at $\nu_3 \sim 2130$ cm^{-1} are decayed. A sharp transmittance appears at $\nu_9 \sim 1050$ cm^{-1} with a broad shoulder in the wave number range of $\nu_{10} \sim 1150$ cm^{-1}. It should be noted that a similar spectrum in the range 850–1300 cm-1 is observed for pSi subjected to the thermal oxidation. But in contrast to thermally oxidized pSi, a significant transmittance at $\nu_3 \sim 934$ cm^{-1} attributed to SiOH groups is observed for cathodically polarized pSi. As the cathode polarization time increases, the transmission bands related to all hydride bonds are attenuated. At the same time, the intensities of bands from internal oxygen bonds ($\nu_8 \sim 2240$ cm^{-1}) and siloxane groups Si–O–Si ($\nu_6 \sim 1100$ cm^{-1}) are enhanced.

We can explain these results in the following way. As discussed above, the cathodic polarization of silicon is accompanied by the reduction of atomic or molecular hydrogen. This process can occur due to adsorbed hydrogen ions or neutral solvent molecules. In either case, the formation of hydrogen in atomic or molecular forms is preceded by the adsorption of particles from the solution. As stated above, in porous silicon, hydrogen already exists as the SiHx groups at the surface of the pore sidewalls [33]. The attack of electrons on SiHx groups leads to the breaking of silicon bonds. Broken silicon bonds are extremely disadvantageous from the thermodynamic point of view. For silicon in the 0.1 M $Er(NO_3)_3$ solution, the oxidation thermodynamic potential by the usual chemical mechanism is considered to be ~1.0 V below the conduction band bottom. Therefore, OH groups and then oxygen rapidly occupy the dangling silicon bonds.

The extended structure of pSi ensures its postreaction oxidation with the formation of internal oxygen bonds. In addition, when pSi is oxidized, the solid phase expands inside the pore increasing the steric factor. Note that the steric factor reflects the fact that there are not only energetic, but also geometric obstacles in the path of the chemical reaction, depending on the geometric structure of the particles and their spatial configuration in the reaction. So, the steric factor is of great importance for the formation of internal oxygen bonds.

Thus, the oxidation and dehydrogenation are typical for pSi during the cathode polarization. These effects should be considered in any cathode polarization of pSi in the solutions, for example, for the cathode cleaning, cathode deposition of foreign materials into pSi, etc.

4. Conclusion

Special conditions for the surface atoms compared to atoms in the crystal bulk are the breaking of the crystal translational symmetry and the formation of dangling bonds. This causes the appearance of allowed energy levels in the band gap. The wave functions of electrons for these levels decay rapidly with distance from the surface, both deep into the crystal and into vacuum. Consequently, these states are characteristic of the surface itself, and the electrons occupying them are located on the surface. The charge due to surface states disrupts the electronic structure inside the semiconductor and induces band bending near the surface. Since at standard conditions the semiconductor crystal should be electrically neutral, the surface charge is compensated by an equal and opposite charge in the near-surface layer. Neutralization occurs due to the attraction to the surface of charge carriers with a sign opposite to the sign of the surface charge, and the repulsion of charge carriers of the same sign. Therefore, the near-surface layer of the semiconductor turns out to be depleted of charge carriers having the same sign as the surface charge, and enriched with carriers of the opposite sign. The thickness of the space charge layer, during which the surface charge is neutralized, depends on the concentration of charge carriers in the semiconductor.

When pSi is placed in an electrolyte, a double electrical layer consisting of an electrical charge on the pSi surface and a charge of ions in the solution at a short distance from the pSi surface is generated at the pSi/solution interface. The charge in this layer is compensated by the supply or removal of electrons in the pSi surface layer to form the space charge layer. This layer has a decisive influence on the electrical conductivity of the silicon skeleton in the pSi layer. Depending on the width, Si elements in pSi may remain practically undepleted, to be partially depleted, or fully depleted. If the silicon skeleton of pSi is undepleted or partially depleted of charge carriers, metal particles nucleate over the entire skeleton surface, including top, side, and pore bottom surfaces. Next, the metal particles are combined into a thin film covering the skeleton. The complete depletion of the pSi skeleton stimulates the electrochemical deposition starting from the pore bottoms and allows the pores to become completely filled with metal.

It has been found that a gel-like erbium-containing deposit is formed during the cathode treatment of pSi in 0.1 M $Er(NO_3)_3$ alcohol solution. The formation of the deposit was shown to take place without the participation of electrons, i.e., the process is not electrochemical but chemical in nature. The formation mechanism of the erbium-containing deposit during the cathode polarization of pSi in the solution of erbium salt is proposed. First, the electrochemical process of the cathode reduction of hydrogen takes place. This process leads to disruption of the ion balance in the cathode space, creating its alkalinization. The alkaline environment favors the

occurrence and development of the chemical reaction of the erbium hydroxide formation. Formed as a gel, erbium hydroxide is physically adsorbed on the cathode surface as a deposit. The deposit composition was found to be $Er(OH)_x(NO_3)_y(C_2H_5O)_z{\cdot}nH_2O$, $x + y + z = 3$, for the pSi cathode polarization in the ethanol solution and $Er^{3+} + OH^- + NO_3^- \rightarrow Er(OH)_x(NO_3)_y$, $x + y = 3$, for the pSi cathode polarization in the aqueous solution of $Er(NO_3)_3$.

The oxidation and dehydrogenation are typical for pSi during the cathode polarization. These effects should be taken into account for any cathode polarization of pSi in the solutions, for example, for the cathode cleaning, cathode deposition of foreign materials into pSi, etc. The obtained results open wide prospects for practical application of Er-filled pSi as a promising material for practical biomedical application as prospective electrodes.

Data availability statement

The datasets generated during and/or analyzed during the current study are available from the corresponding author on reasonable request.

CRediT authorship contribution statement

V. Yakovtseva: Writing – original draft, Supervision, Investigation, Formal analysis. **S. Volchek:** Supervision, Project administration, Funding acquisition. **V. Bondarenko:** Writing – original draft, Supervision, Methodology, Conceptualization. **M.I. Sayyed:** Writing – review & editing, Visualization. **Taha A. Hanafy:** Writing – review & editing. **S. Trukhanov:** Writing – review & editing. **A. Bondaruk:** Writing – review & editing, Visualization. **A. Rotkovich:** Writing – review & editing, Software. **M.V. Silibin:** Methodology, Investigation. **T. Zubar:** Writing – original draft. **D. Tishkevich:** Writing – review & editing, Writing – original draft. **A. Trukhanov:** Writing – review & editing, Writing – original draft.

Declaration of competing interest

The authors declare that they have no known competing financial interests or personal relationships that could have appeared to influence the work reported in this paper.

Acknowledgments

The work was carried out as part of a major scientific project with financial support from the Russian Federation represented by the Ministry of Science and Higher Education of the Russian Federation under agreement No. 075-15-2024-555 dated April 25, 2024. M.S. acknowledges the Academic leadership program Priority 2030 proposed by Federal State Autonomous Educational Institution of Higher Education I.M. Sechenov First Moscow State Medical University of the Ministry of Health of the Russian Federation (Sechenov University). The belarusian part thanks to grants 4.1.5 of the Belarus State Program for the Scientific Research “Material science, new materials and technologies” and 3.6 of the Belarus State Program for the Scientific Research “Photonics and electronics for innovation”.

References

[1] R. Herino, Nanocomposite materials from porous silicon, Mater. Sci. Eng. B 69 (2000) 70–76.
[2] G.L. Drisko, C. Sanchez, Hybridization in materials science – evolution, current state, and future aspirations, Eur. J. Inorg. Chem. (2012) 5097–5105.
[3] L.T. Canham (Ed.), Handbook of Porous Silicon, Springer International Publishing Switzerland, 2014, p. 1613.
[4] V. Lehman, Electrochemistry of Silicon: Instrumentation, Science, Materials and Applications, Wiley-VCH, Weinheim, 2002, p. 277.
[5] M.J. Sailor, Porous Silicon in Practice: Preparation, Characterization and Applications, Wiley-VCH, Weinheim, 2012, p. 262.
[6] Properties of Porous Silicon, in: L.T. Canham (Ed.), IEE Books, EMIS Datareviews Series, № 18, first ed.INSPEC, The Institution of Electrical Engineers, London. United Kingdom, 1997, p. 424.
[7] G. Korotcenkov (Ed.), Porous Silicon: from Formation to Application, Vols. 1-3, first ed., Taylor and Francis Group, CRC Press, Boca Raton, USA, 2016, p. 1286.
[8] P. Granitzer, K. Rumpf, Porous silicon—a versatile host material, Materials 3 (2010) 943–998.
[9] V. Yakovtseva, L. Dolgyi, N. Kazuchits, N. Vorozov, M. Balucani, V. Bondarenko, L. Franchina, G. Lamedica, A. Ferrari, Oxidized porous silicon: from dielectric isolation to integrated optical waveguides, J. Porous Mater. 7 (2000) 215–222.
[10] Y. Ogata, K. Kobayashi, M. Motoyama, Electrochemical metal deposition on silicon, Curr. Opt.Sol. St. Mater. Sci. 10 (2006) 163–172.
[11] V. Petrovich, S. Volchek, L. Dolgyi, V. Yakovtseva, N. Kazuchits, V. Bondarenko, L. Tsybeskov, P. Fauchet, Deposition of erbium containing film in porous silicon from ethanol solution of erbium salt, J. Porous Mater. 7 (2000) 37–40.
[12] V. Petrovich, S. Volchek, L. Dolgyi, V. Yakovtseva, V. Bondarenko, M. Balucani, G. Lamedica, A. Ferrari, T. Benson, H. Arrand, Formation features of deposits during a cathode treatment of porous silicon in aqueous solutions of erbium salts, J. Electrochem. Soc. 147 (2000) 655–658.
[13] A.I. Vorobjova, D.L. Shimanovich, O.A. Sycheva, T.I. Ezovitova, D.I. Tishkevich, A.V. Trykhanov, Studying the thermodynamic properties of composite magnetic material based on anodic alumina, Rus. Microelectron. 48 (2019) 107–118.
[14] M. Balucani, P. Nenzi, E. Chubenko, A. Klyshko, V. Bondarenko, Electrochemical and hydrothermal deposition of ZnO on silicon: from continuous films to nanocrystals, J. Nanoparticle Res. 13 (2011) 5985–5997.
[15] H. Bandarenka, A. Dolgiy, E. Chubenko, S. Redko, K. Girel, S. Prischepa, A. Panarin, S. Terekhov, V. Pilipenko, V. Bondarenko, Nanostructured metal films formed onto porous silicon template, J. Nano Res. 39 (2016) 235–255.
[16] N. Grevtsov, E. Chubenko, V. Bondarenko, I. Gavrilin, A. Dronov, S. Gavrilov, Electrochemical deposition of indium into oxidized and unoxidized porous silicon, Thin Solid Films 734 (2021) 138860.
[17] N. Grevtsov, E. Chubenko, V. Petrovich, V. Bondarenko, I. Gavrilin, A. Dronov, S. Gavrilov, Selective electrochemical deposition of indium in-between silicon nanowire arrays fabricated by metal-assisted chemical etching, Materialia 21 (2022) 101337.

[18] N. Grevtsov, E. Chubenko, V. Bondarenko, I. Gavrilin, A. Dronov, S. Gavrilov, Germanium electrodeposition into porous silicon for silicon-germanium alloying, Materialia 26 (2022) 101558.
[19] N. Grevtsov, E. Chubenko, V. Bondarenko, I. Gavrilin, A. Dronov, S. Gavrilov, G. Rymski, K. Yanushkevich, D. Goroshko, E. Argunov, Composition-adjustable silicon-germanium alloy films based on porous silicon, Mater. Today Commun. 38 (2023) 107886.
[20] T. Kimura, A. Yokoi, H. Horiguchi, R. Saito, T. Ikoma, A. Sato, Electrochemical Er doping of porous silicon and its room-temperature luminescence at ~1.54 μm, Appl. Phys. Lett. 65 (1994) 983–985.
[21] E.S. Marstein, J.K. Skjelnes, T.G. Finstad, Incorporation of erbium in porous silicon, Phys. Scripta T101 (2002) 103–105.
[22] M.E. Castagna, A. Muscara, S. Leonardi, S. Coffa, L. Caristia, C. Tringali, S. Lorenti, Si-based erbium doped light-emitting devices, J. Lumin. 121 (2) (2006) 187–192.
[23] H. Omar, N.K. Sabri, A.A.S.M. Radzi, M. Rusop, S. Abdullah, N.I. Ikhsan, Optical characterization of porous silicon (PS) doped erbium (Er) using photoluminescence spectroscopy, Adv. Mater. Res. 832 (2014) 617–621.
[24] G. Mula, S. Setzu, G. Manunza, R. Ruffilli, A. Falqui, Characterization of Er in porous Si, Nanoscale Res. Lett. 7 (2012) 376.
[25] G. Mula, L. Loddo, E. Pinna, M.V. Tiddia, M. Mascia, S. Palmas, R. Ruffilli, A. Falqui, Controlling the Er content of porous silicon using the doping current intensity, Nanoscale Res. Lett. 9 (2014) 332.
[26] M. Pourbaix, Atlas of Electrochemical Equilibria in Aqueous Solutions, 2nd English ed., Publisher: National Association of Corrosion Engineer, 1974, p. 645.
[27] Techniques of Chemistry: 3 Volumes; Yeager E., Salkind A.J., Eds.; Wiley-Interscience: New York, 1972, vol. 1, 581 p.
[28] I. Tamm, On the possible bound states of electrons on a crystal surface, Phys. Z. Sowjetunion 1 (1932) 73.
[29] K. Oura, V.G. Lifshits, A.A. Saranin, A.V. Zotov, M. Katayama, Surface science: an introduction, in: 1st ed.; Spriger-Verlag, Berlin Heidelberg New York, 2003, p. 440.
[30] H.H. Girault, in: J.O.'M. Bockris, B.E. Conway, R.E. White (Eds.), Modern Aspects of Electrochemistry, vol. 25, Plenum: N.Y.: Springer Science+Business Media, New York, 1993, p. 333.
[31] Groß A, Theoretical Surface Science, Springer-Verlag Berlin Heidelberg, 2009, p. 342.
[32] M.J. Sailor, Chemical reactivity and surface chemistry of porous silicon, in: L.T. Canham (Ed.), Handbook of Porous Silicon, Springer International Publishing Switzerland, 2014, pp. 355–380.
[33] P. Gupta, A.C. Dillon, A.S. Bracker, S.M. George, FTIR studies of H_2O and D_2O decomposition on porous silicon, Surf. Sci. 245 (1991) 360–372.
[34] S.M. Sze, Kwok K. Ng, Physics of Semiconductor Devices, third ed., A John Wiley & Sons, Inc., Hoboken, New Jersey, 2006, p. 815.
[35] P.J. Boddy, W.H. Brattain, The distribution of potential at the germanium – aqueous electrolyte interface, J. Electrochem. Soc. 110 (1963) 570.
[36] H. Gerischer, Electrochemistry of semiconductors, in: H. Eyrving (Ed.), Phisical Chemistry, 9a, Academic Press, New York-London, 1970, p. 463.
[37] S.L. Prischepa, A.L. Dolgiy, H.V. Bandarenka, V.P. Bondarenko, K.I. Yanushkevich, V.G. Bayev, A.A. Maximenko, YuA. Fedotova, A. Zarzycki, Y. Zabila, Synthesis and properties of Ni nanowires in porous silicon tempaltes, in: L.J. Wilson (Ed.), Nanowires: Synthesis, Electrical Properties and Uses in Biological Systems, Nova Science Publishers, New York, 2014, pp. 89–129.
[38] A. Dolgiy, S. Redko, H. Bandarenka, S. Prischepa, K. Yanushkevich, P. Nenzi, M. Balucani, V. Bondarenko, Electrochemical deposition and characterization of Ni in mesoporous silicon, J. Electrochem. Soc. 159 (10) (2012) D623–D627.
[39] A. Dolgyi, H. Bandarenka, S. Prischepa, K. Yanushkevich, P. Nenzi, M. Balucani, V. Bondarenko, Electrochemical Deposition of Ni into Mesoporous Silicon, vol. 41, Electrochemical Society Transactions, 2012, pp. 111–118.
[40] D.A. Atwood, *The Rare Earth Elements Fundamentals And Applications*; Publisher, John Wiley & Sons Ltd, West Sussex, UK, 2012, p. 629.
[41] A.J. Bard, L.R. Faulkner, Electrochemical Methods: Fundamentals and Applications, second ed., Publisher: Wiley, New York, 2001, p. 850.
[42] S. Cotton, *Lanthanide And Actinide Chemistry;* Publisher, John Wiley & Sons, 2013, p. 288.